Engineered Science

RESEARCH PAPER View Article Online

Catalytic Degradation of 4-Nitrophenol in Polluted Water by Three-Dimensional Gold Nanoparticles/Reduced Graphene Oxide Microspheres

Ning Li,[1,2] Fuhua Zhang,[1,2] Hua Wang[2*] and Shifeng Hou[1,2*]

Microspheres as catalysts catalyst supports have attracted a great deal of attention over the last two decades. Here, gold nanoparticles (Au-NPs) encapsulated within the reduced graphene oxide microspheres (rGO microspheres) were prepared by using a spray-drying method. The Au-NPs were distributed evenly through the rGO microsphere composite. The mass content of Au-NPs in the rGO microspheres composite reached 30.3%, and the average size of the Au-NPs was 10.5±2.5 nm. The morphologies and structural characteristics of the materials were determined by scanning electron microscopy (SEM), transmission electron microscopy (TEM), high-resolution transmission electron microscopy (HRTEM) and X-ray diffraction (XRD) patterns. The as-prepared composite was used to catalyze the reduction of 4-nitrophenol to 4-aminophenol in the presence of excess sodium borohydride and exhibited high catalytic activity. The catalysis process was monitored by UV spectroscopy, and the first order rate constant of the catalytic reaction K was 1.96×10^{-3} s^{-1}, and the activation energy E_a was found to be 3.5×10^4 J/mol. The catalytic experiment results indicated the Au/rGO microspheres prepared have a great application for friendly environment aspects.

Keywords: Gold Nanoparticles; Reduced Graphene Oxide Microspheres; 4-nitrophenol; Catalytic Reduction

Received 8 January 2019**, Accepted** 15 March 2019

DOI: 10.30919/es8d509

1. Introduction

In recent years, the treatment technique of the pollution of water by phenol compounds has attracted widespread attention. Industrial production of pesticides, paints, and drugs produces 4-nitrophenol (4-NP), which is both difficult to degrade and toxic. 4-aminophenol (4-AP) is a catalytic product of 4-NP and is less toxic than 4-NP, and thus to convert 4-NP into 4-AP is an ideal choice.[1-3] At present, the commonly used methods for removing 4-NP are adsorption, microbial degradation, photocatalytic degradation, electrocoagulation and electrochemical methods.[4-7] Although the above methods have certain effects on the removal of 4-NP, they have some limitations, such as inefficient degradation, slow degradation and secondary pollution. Additionally, the operating costs, reaction conditions and equipment also have higher requirements. The hydrogenation method has the advantages of being mild, efficient, rapid, and environmentally friendly, meeting the "green chemistry" concept.[8-10] Commonly used catalysts include noble metals (Au, Pt, Pd, Ru, Rh) and non-precious metals (Ag, Cu, Ni, Fe, Mn).[11-20] Au nanoparticles (Au-NPs) have more efficient catalytic activity under mild conditions.[21] The conversion of 4-NP to 4-AP catalyzed by Au-NPs in sodium borohydride solution ($NaBH_4$) has been extensively studied. However, Au-NPs have a large specific surface area and very high surface energy, which lead to agglomeration. Once Au-NPs agglomerate, their catalytic activity decreases. While ensuring high catalytic activity sites, it is extremely important to prevent the agglomeration of Au-NPs.[22-25] To inhibit the agglomeration of Au-NPs, they were loaded on carriers of various morphologies and compositions. Spherical nanocomposites prepared by the spherical carrier have the advantages of a high specific surface area, excellent diffusion properties and easily modified surfaces on the spherical nanostructures.[26-27] Catalytic materials prepared with spherical carriers not only exhibit high activity and high stability to target reactions but also are recyclable, while the inorganic type of spherical carrier also has high temperature resistance, anti-aging properties, etc.[28-29] There are a number of spherical substrates supported Au-NPs that catalyze the reduction of 4-NP. For example, Dong *et al.*[30] synthesized Au-NPs loaded with polysilsesquioxane, which was used as catalyst in the reduction of 4-NP. There was no by-product in the reduction of 4-NP, and the conversion rate reached 97.8% in 60 minutes. After centrifugal recovery and 10 cycles, the conversion rate remained at 95.1%.

Graphene is a newly discovered two-dimensional carbon material with a very large surface area, good electrical conductivity, and high electron transport capacity.[31-32] The Au-NPs dispersed in graphene can not only guarantee that Au-NPs reassemble together but also use a large specific surface of the graphene to bring the material into full contact with the waste liquid. For example, Vellaichamy *et al.*[33] synthesized AuNPs@RGO nanosheets. Although it has a good reducing effect on 4-nitrophenol, but still cannot solve the problem of reduced catalytic degradation efficiency due to agglomeration of AuNPs. Further, the problem with graphene material is that the two-dimensional graphene sheet has a large surface area to easily reunite into a bulk piece by Van der Waals force and π-π stacking.[34] The two-dimensional graphene being made into three-dimensional can be a good solution to this problem.

In this study, we fabricate Au-NPs supported on reduced graphene (Au-NPs/rGO) microspheres to form composites for the efficient

[1] *School of Chemistry and Chemical Engineering, Shandong University, Jinan, Shandong 250100, China*

[2] *National Engineering and Technology Research Center for Colloidal Materials, Shandong University, Jinan, Shandong 250100, China*

***E-mail:** h.wang@sdu.edu.cn*

catalytic degradation of 4-NP. The Au-NPs/rGO microsphere composites were prepared by spray-coating followed by high-temperature thermal reduction. It was found that Au-NPs/rGO microsphere composites showed an outstanding catalytic performance towards 4-nitrophenol to 4-aminophenol. AuNPs/rGO microspheres are effective catalyst for 4-NP reduction in the presence of $NaBH_4$, and the catalytic process was detected by UV-Visible spectrum. The catalytic effect and recyclability of Au-NPs/rGO microspheres for 4-NP in polluted water are superior to those of conventional catalyst materials.

Compared with Au-NPs/rGO lamellae material, several advantages of as-prepared Au-NPs/rGO microspheres to catalyze the reduction of 4-Nitrophenol are as follows. (i) The high specific surface area of the three-dimensional microsphere structure with the cell as a natural model provides more active sites for the Au-NPs, which facilitates sufficient contact between the catalyst and the waste liquid and the progress of the catalytic process. (ii) The microsphere structure can effectively stabilize and disperse the gold nanoparticles, stabilize the particles against aggregation, and increase the catalytic reduction rate. (iii) Compared with ordinary bulk two-dimensional graphene, the three-dimensional graphene microspheres have small volume, excellent dispersion performance and stability, and are beneficial to improve the stability and recycling of the graphene-based catalyst.[35]

2. Experimental section

2.1. Chemicals

Graphite oxide (GO) was provided by Jining Leadernano Co., Ltd. (Jining, China). 4-Nitrophenol (4-NP) and sodium borohydride were supplied by Sinopharm Chemical Reagent Co., Ltd. (Shanghai, China). Chloroauric acid ($HAuCl_4 \cdot 4H_2O$) and trisodium citrate were provided by the Sinopharm Group Chemical Reagent Co., Ltd. All reagents were analytical grade and were used directly without further treatment. All aqueous solutions were prepared with deionized water with a resistivity of 18.25 MΩ·cm.

2.2. Sample preparation

2.2.1. Preparation of gold nanoparticles (Au-NPs)

The chloroauric acid was used to prepare into a 24.28 mM $HAuCl_4$ solution. In a typical synthesis, 100 mL of the $HAuCl_4$ solution was placed in a three-necked flask and heated to reflux for 3 minutes. Then 80 mL of a 10% trisodium citrate solution containing 0.34 g of polyvinylpyrrolidone (PVP) was quickly injected and the solution was further boiled for 10 minutes. Magnetic stirring was maintained for the entire reaction period, until cool to room temperature, at which point the solution was stored in the refrigerator at 4 °C for use.

2.2.2. Synthesis of Au-NPs/rGO microspheres and Au-NPs/rGO lamellae composites

The Au-NPs/rGO microspheres were synthesized by using a spray-drying method as illustrated in previously reported procedures with slight modification.[36] In a standard procedure, 5.0 mg/mL GO solution was mixed with the Au-NPs solution and sonicated for 3 hours to ensure even mixing. The Au-NPs/GO precursor solution, with a mass ratio of $HAuCl_4$ to GO of 1:1, was spray-dried and collected to heat at 500 ℃ in a tube furnace under nitrogen atmosphere. Over the thermal reduction process, the samples were cooled down to room temperature naturally. Products were rinsed with ultra-pure water several times, then dried and stored for future usage. The Au-NPs/rGO lamellae material was synthesized in the manner described above, except that the spray-drying method was changed into the freeze-drying method.

2.3. Apparatus

The BILON-6000Y spray-dryer (Shanghai Bilang Instrument Manufacturing Co. Ltd., China) was used for spray-drying to obtain Au-NPs/rGO microspheres composites. The CF-16RN centrifuge (Hitachi kokl Co. Ltd, Tokyo Japan) was used for centrifugation to obtain a catalyzed solution. The morphology of the composites was obtained by a SU8010 microscope (3.0 kV scanning electron microscopy [SEM] HITACHI, Tokyo, Japan), a JEM-1011 microscope (200 kV transmission electron microscopy [TEM] JEOL, Tokyo, Japan) and a JEM-2100 microscope (200 kV high-resolution transmission electron microscopy [HRTEM] JEOL, Tokyo, Japan). The structural characteristics of the samples were characterized by filtered Cu Kα, λ=0.154 nm X-ray diffraction (XRD) patterns and Raman spectrometer (PHS-3C, Horbin, France) with excitation of 633 nm laser. The UV spectrum was measured by a TU-1901 UV-Visible Spectrophotometer (PERSEE, Beijing, China). The content of the material components was obtained by measuring diamond TG / DTA thermogravimetric analysis (Perkin Elmer, America) using air as the process gas, a gas flow rate of 20 sccm, and a heating rate of 10 °C/min.

2.4. Catalytic properties

The catalytic reduction properties of the 4-nitrophenol with as-prepared catalyst were investigated by adding 0.1 mL of 4-nitrophenol aqueous solution (4.0 mM) into 5.0 mL distilled water solution. A certain amount of AuNPs/rGO microsphere (1.0 mg/mL) was added to the solution, and then 0.4 mL of fresh $NaBH_4$ aqueous solution (0.12 M) was added to above solution and the stop-watch was used to immediately to record the reaction time. The solution was then filled quickly at a giving time or centrifuged for 2 minutes (14000 r/min), and the above solution was used to fill a cuvette for testing with UV-VIS.

During the catalytic reaction, 4-NP was converted to 4-AP, and then the absorbance of 4-nitrophenol at 400 nm will decrease. The absorbance of 4-nitrophenol at 400 nm is proportional to its concentration, so the concentration ratio of 4-nitrophenol at the giving time (C_t) to the initial concentration (C_0), C_t/C_0 will be equal to the ratio of absorbance intensity at giving time t_t (A_t) to that at start t_0 (A_0). As a result, the progress of the reaction could be directly reflected by the change of the Ultraviolet absorption intensity of 4-NP and 4-AP.

3. Results and discussions

3.1. Morphology and structure of the Au-NPs/rGO microspheres

The detail morphology structures of the Au-NPs/rGO microspheres were depicted in Fig. 1. Fig. 1a, b and c depicted the SEM and TEM image of Au-NPs/rGO microspheres, it can be seen that a well-defined microsphere structure were obtained with rGO sheet as the microsphere and the Au-NPs distributed within the microsphere entirely. From Fig. 1b, the Au-NPs with a lattice spacing of 0.23 nm (inset of Fig. 1d) were found to be uniformly dispersed in the graphene material, and Fig. 1d showed the size of the Au-NPs, which average to (10.5±2.5) nm (inset of Fig. 1d). As a control experiment, the Au-NPs/rGO materials prepared by the freeze-drying method have sheet structures (shown in Figs S1a and b). To further demonstrate the uniform distribution of Au-NPs in Au-NPs/rGO microspheres, we have performed mapping of the image in Fig. 2. It can be seen that the Au-NPs are distributed evenly throughout the microsphere without aggregation.

In order to further determine the successful synthesis of Au-NPs/rGO microspheres, Raman and XRD were also implemented. Fig. 3 showed Raman spectra of GO, rGO, Au-NPs/rGO microspheres and Au-NPs/rGO lamellae. Au-NPs/rGO microspheres and Au-NPs/rGO lamellae have similar Raman peak characteristics corresponding to the

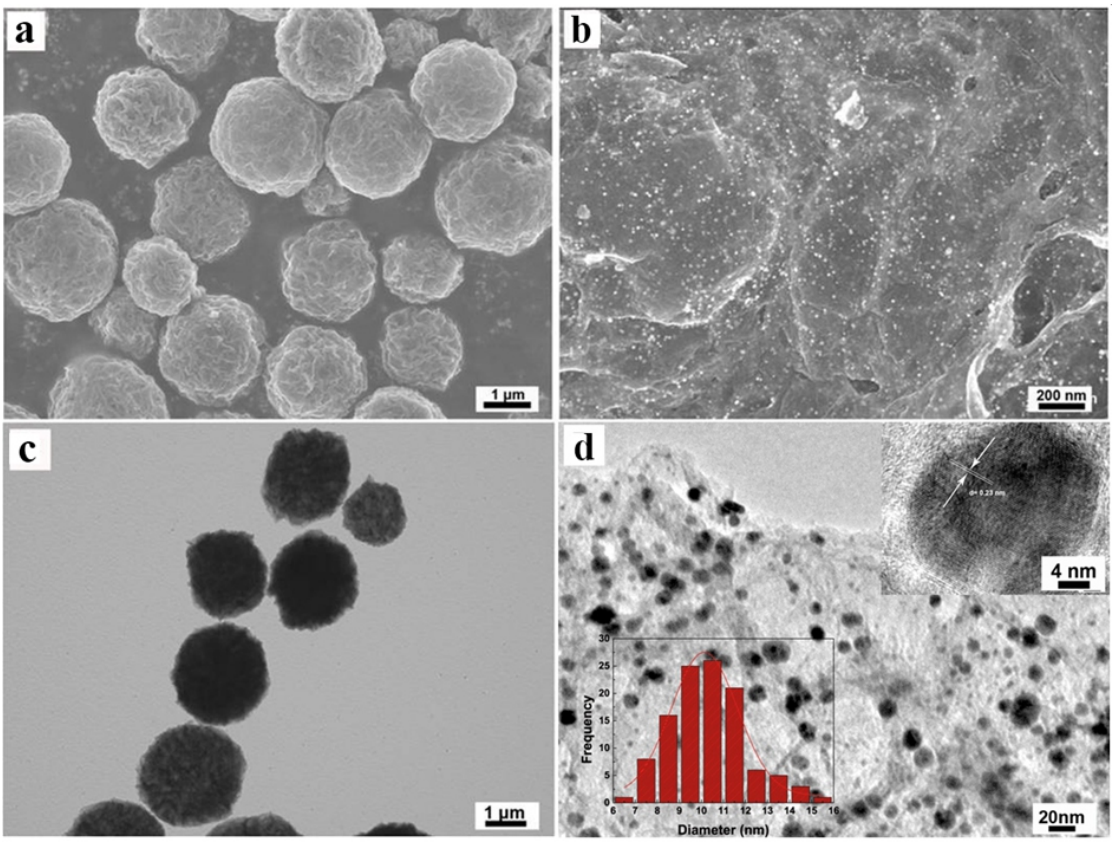

Fig. 1 (a), (b) SEM and (c) TEM images of Au-NPs/rGO microspheres, (d) HRTEM image of Au nanoparticles of Au-NPs/rGO microspheres, the inset is a single Au nanoparticle of Au-NPs/rGO microspheres and average particle size distribution.

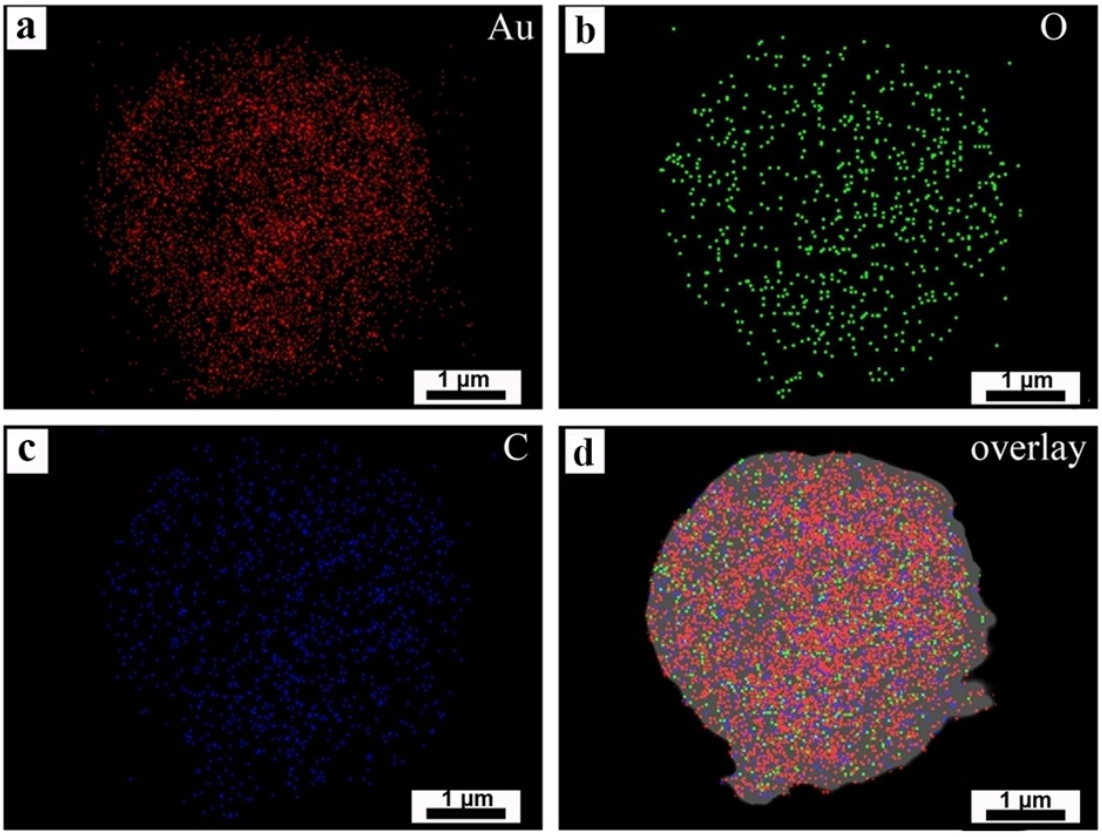

Fig. 2 The mapping of Au-NPs/rGO microspheres.

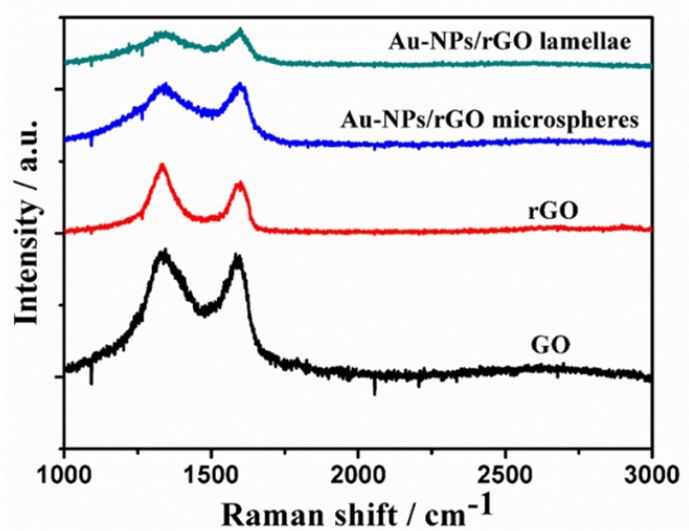

Fig. 3 Raman spectra of GO, rGO, Au-NPs/rGO microspheres, Au-NPs/rGO lamellae.

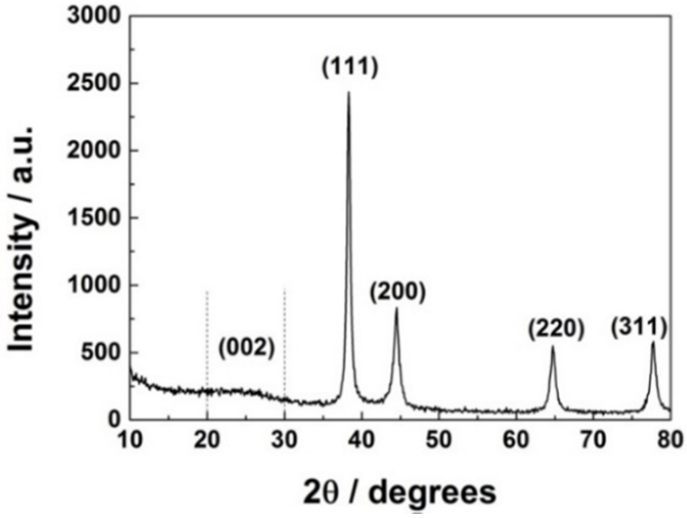

Fig. 4 The diffraction pattern of the Au-NPs/rGO microspheres.

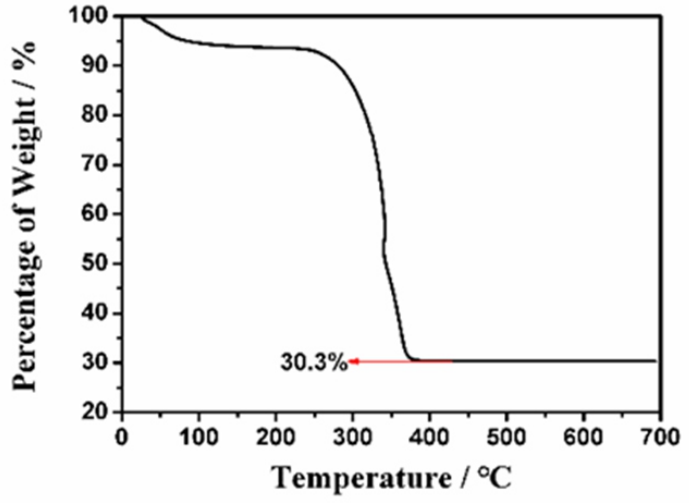

Fig. 5 Thermogravimetric curve of Au-NPs/rGO microspheres.

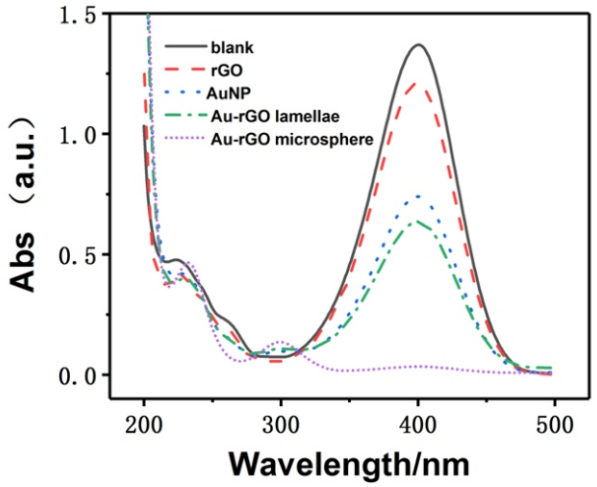

Fig. 6 UV spectrum of blank solution, rGO, Au-NPs, the Au-NPs/rGO lamellae, Au-NPs/rGO microspheres in 20.0M 4-NP, 400.0M $NaBH_4$ at 298 K for 30 minutes.

Table 1 Specific surface area and pore structure of the Au-NPs/rGO materials studied.

Material	BET surface area (m^2 g^{-1})	Pore volume (cm^3 g^{-1})	t-Plot		
			Micropore area (m^2 g^{-1})	External surface area (m^2 g^{-1})	t-Plot micropore volume (cm^2 g^{-1})
Au-NPs/rGO microspheres	230.4	0.28	167.6	62.9	0.062
Au-NPs/rGO lamellae	146.7	0.11	108.2	38.5	0.047

D (1344 cm^{-1}) and G (1583 cm^{-1}) bands of GO and rGO.[37] By comparing the $I_D/I_{G(rGO)}$=1.4, $I_D/I_{G(Au\text{-}NPs/rGO\ microspheres)}$=1, $I_D/I_{G(Au\text{-}NPs/rGO\ lamellae)}$=1.03 and peak shape curve, it can be roughly obtained that the addition of Au-NPs has a certain influence on the Raman peak of Au-NPs/rGO microspheres and Au-NPs/rGO lamellae, indicating that the Au-NPs on the surface and internal nucleation of rGO will bring additional defects to the structure. Fig. 4 displayed the XRD pattern of Au-NPs/rGO microspheres, which showed four peaks at about 38.4, 44.6, 64.8, and 77.9°, corresponding to the (111), (200), (220), (311) crystal faces of the face-centred cubic structure of crystalline Au ((JCPDS file card no. 04-0784), respectively. And 20-30° wide C peak indexed to the (002) crystal face of graphene.[38] According to Scherrer's Formula, the average size of Au-NPs was about 11 nm, which is consistent with the result of TEM.

The gold content of the synthesized material was further confirmed by the thermogravimetric analysis. A typical thermogravimetric curve in Fig. 5 showed that the content of gold nanoparticles in the composites was 30.3 wt%, which was in accordance with the theoretical designed 33.3 wt%, demonstrated that a high loading of non-agglomerated Au-NPs within the graphene made by the spray-drying method.

The total pore volume and the Brunauer Emmett Teller (BET) specific surface area of Au-NPs/rGO microsphere are 0.28 $cm^3\ g^{-1}$ and 230.4 $m^2\ g^{-1}$, respectively, which are much higher than that of freeze-dried rGO sample (Table 1). Au-NPs/rGO microspheres have a large specific surface area, provide a larger contact site with 4-NP, and facilitate the uniform dispersion of Au-NPs to provide sufficient catalytic sites to increase the rate of catalytic degradation to 4-NP. The reason for the analysis may be that graphene microspheres are beneficial to maintaining a three-dimensional multi-space network, and the flaky graphene sample prepared by lyophilization tends to collapse the pores and fail to provide a high specific surface area.

3.2. Catalytic reduction of 4-NP to 4-AP

The catalytic properties of the catalyst toward the reduction of 4-NP in the excess of $NaBH_4$ were then investigated by UV-vis spectra. The UV spectrum in Fig. 6 showed the catalytic process of rGO, Au-NPs, Au-NPs/rGO lamellae, and Au-NPs/rGO microspheres towards the reduction in 20.0 M 4-NP, 400.0 M $NaBH_4$ at 298 K. The UV spectrum at 400 nm was the 4-NP ion absorption peak. With 4-NP conversion to 4-AP, the UV absorption peak at 400 nm gradually decreased, while the UV absorption peak associated with 4-AP appeared at 290 nm.[39] As we can see from the UV-vis spectrum, rGO did not have a catalytic effect as the blank solution, but there is a slight adsorption of 4-NP. The catalytic effect of Au-NPs/rGO lamellae was weaker than that of the Au-NPs solution. However, the catalytic effect of Au-NPs /rGO microspheres was better than that of the Au-NPs solution.

To compare the catalytic effects of Au-NPs/rGO microspheres and Au-NPs/rGO lamellae, we placed 0.5 mL of Au-NPs/rGO microsphere suspension (1.0 mg/mL) into 0.1 mL 4.0 mM 4-NP, 0.4 mL 120.0 mM $NaBH_4$, and 5 mL deionized water at 298 K. The UV-vis spectra of the reaction process were depicted in Fig. 7a and b. It can be seen from the Fig. 7 that the Au-NPs/rGO microsphere material can convert the 4-NP to 4-AP entirely within 28 minutes, and the Au-NPs/rGO lamellae material did so with at least 140 minutes. The catalyst received the electron donor BH_4^-, then transferred to the electron acceptor of 4-NP, and thus the catalytic reaction occurred.[40] Since $NaBH_4$ was in excess, it could be considered that the reduction rate was independent of the $NaBH_4$ content. $NaBH_4$ was added to the 4-NP solution to form a 4-NP ion, and the color of the solution changed from pale yellow-green to dark yellow-green.

Fig. 7c was a linear correlation between $\ln(A_t/A_0)$ and reaction time (T) (A_t was the intensity of the absorption peak after a certain time t, and A_0 was the intensity of the absorption peak at the beginning), indicating that the reaction was a pseudofirst-order reaction.[41] The Au-NPs/rGO microspheres had a pseudofirst-order rate constant of K_{app}= -$1.96\times10^{-3}\ s^{-1}$, which was much higher than the Au-NPs/rGO lamellae material's K_{app}= -$0.36\times10^{-3}\ s^{-1}$. We also calculated the ratio of the rate constant K to the weight of Au-NPs in the catalyst, $K_{app}/m=K/m=12.94\ s^{-1}g^{-1}$. Table 2 showed a comparison of Kapp and Kapp/m of different catalytic systems for the reduction of 4-NP (298 K). It could be found that the Au-NPs/rGO microsphere prepared in this work had the highest catalytic activity. One reason was that the microsphere structures can improve the mass transfer as compared to the same mass of lamellae supported catalysts. And the microsphere structure of graphene provided specific surface area, which can be effective for adsorbing 4-NP by π-π conjugation and the free space within the microsphere provided more space for the 4-NP to reach the catalytic sites.[42-43] Another reason was that the microsphere structures can prevent the leaking and aggregation of gold nanoparticles, which can provide more catalytic activity sites to 4-NP and thus can stabilize the gold nanoparticles during the reaction process.

To test the influence of the amount of catalyst on the catalytic behavior, we added 0.25 mL, 0.5 mL, and 0.75 mL of Au-NPs/rGO solution (1.0 mg/mL) to 6.0 mL reaction solution of 0.4 mol 4-NP and

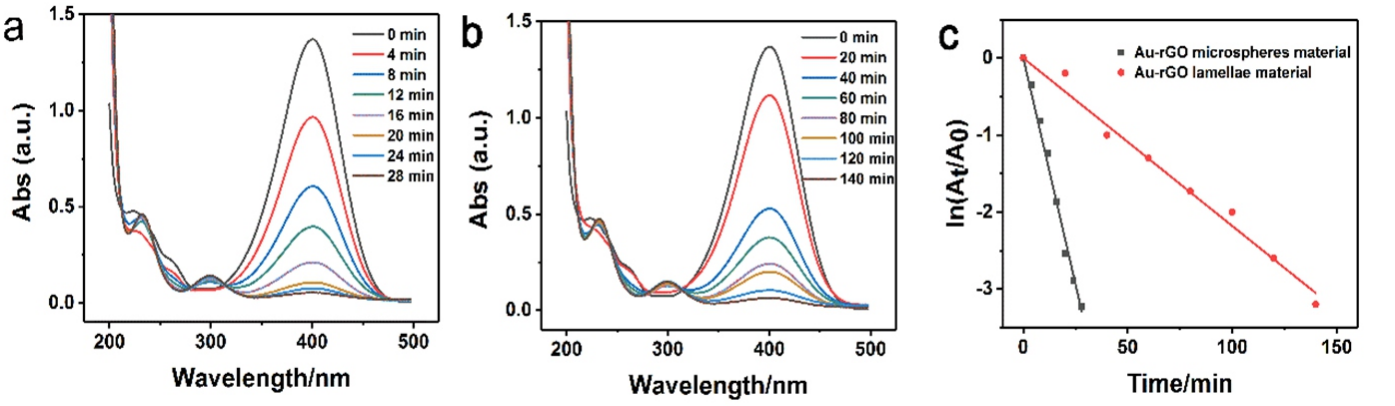

Fig. 7 UV spectrum of (a) Au-NPs/rGO microspheres; (b) Au-NPs/rGO lamellae in 0.4 mol 4-NP, 48.0 mol $NaBH_4$ at 298 K; (c) the relation of t vis ln (A_t/A_0).

48.0 mol $NaBH_4$, and the results were depicted in Fig. 8. Fig. 8c shows a linear correlation between ln (A_t/A_0) and T of 0.25 mL, 0.5 mL, and 0.75 mL of microspheres (1.0 mg/mL). Pseudofirst-order rate constants were $K_{0.25}$=-1.25×10^{-3} s^{-1}, $K_{0.5}$=-1.96×10^{-3} s^{-1}, and $K_{0.75}$=-3.13×10^{-3} s^{-1}. The corresponding K_{app}/m is $K_{0.25}$/m=16.5 s^{-1}g^{-1}, $K_{0.5}$/m=12.94 s^{-1}g^{-1}, $K_{1.5}$/m=13.77 s^{-1}g^{-1} respectively. It can be seen that K increased with the increasing concentration of catalyst. This was because as the amount of catalyst increases, the amount of catalysis site of the catalyst increased, leading to an increase in K, but the reaction rate of per mass of AuNPs is basically unchanged, resulting in K_{app}/m staying constant roughly.

The effect of temperature on the reduction of 4-NP with $NaBH_4$ in the presence of Au-NPs/rGO microspheres at different temperature was shown in Fig. 9a and b, and a linear correlation between ln (A_t/A_0) and T across 273, 298 and 323 K displayed in Fig. 8c. The values of the pseudofirst-order rate constants were $K_{273\ K}$ = -0.34×10^{-3} s^{-1}, $K_{298\ K}$ = -1.96×10^{-3} s^{-1}, and $K_{323\ K}$= -3.55×10^{-3} s^{-1}. According to the relationship between temperature and pseudofirst-order rate constants, we can calculate the activation energy Ea = 3.5x10^4 J/mol by the Arrhenius equation.

The catalytic stability of the as-prepared Au-NPs/rGO microspheres was then examined. In a typical experiment, 0.5 mg of the catalyst were added into 0.1 mL 4.0 mM 4-NP solution at 298 K. After 20 minutes,

Table 2 Comparison of K_{app} and K_{app}/m of different catalytic systems for the reduction of 4-NP (298 K).

Support	Catalyst usage [wt%]	$NaBH_4$ (equiv.)	K_{app} (s^{-1})	K_{app}/m (s^{-1}g^{-1})	Ref.
Au/PTSC	33.50	excess	1.60 × 10^{-4}	3.34	44
graphene/PDA–Au Nps	-	-	3.75 × 10^{-3}	3.0	45
Fe_3O_4@CeO_2/Au	1.35	80	1.53 × 10^{-3}	56.67	46
hybrid Au–GO nanocomposites	62	excess	2.06 × 10^{-3}	8.37	47
C/Au/TiO_2	0.86	-	8.7× 10^{-3}	10.08	48
PS-AuNP	4.7	excess	2.75 × 10^{-4}	9.7	49
Au-NPs/rGO microsphere	30.3	excess	1.96 × 10^{-3}	12.94	This work

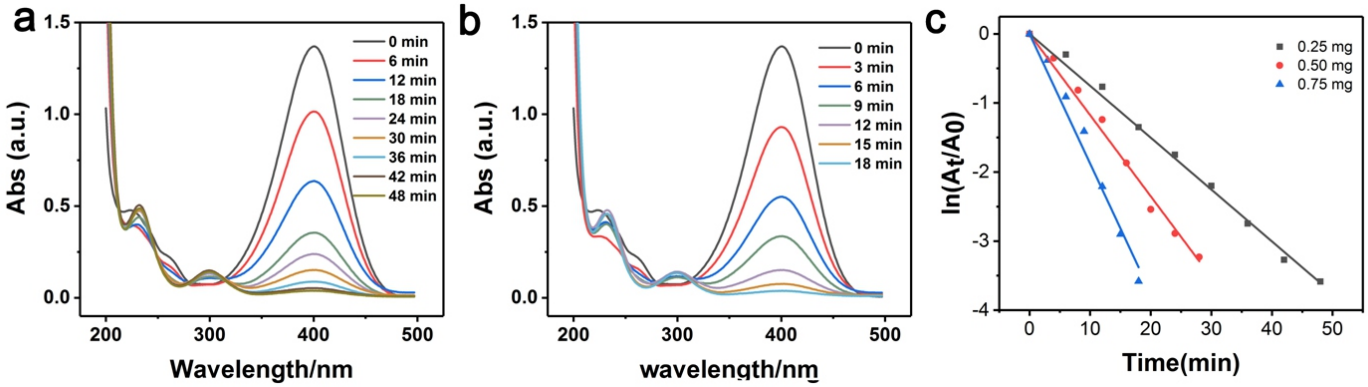

Fig. 8 UV spectrum of (a) 0.25 mg, (b) 0.75 mg of Au-NPs/rGO microspheres in 0.4 mol 4-NP and 48.0 mol $NaBH_4$ at 298 K, and the relation of t vis ln (At/A_0) (c).

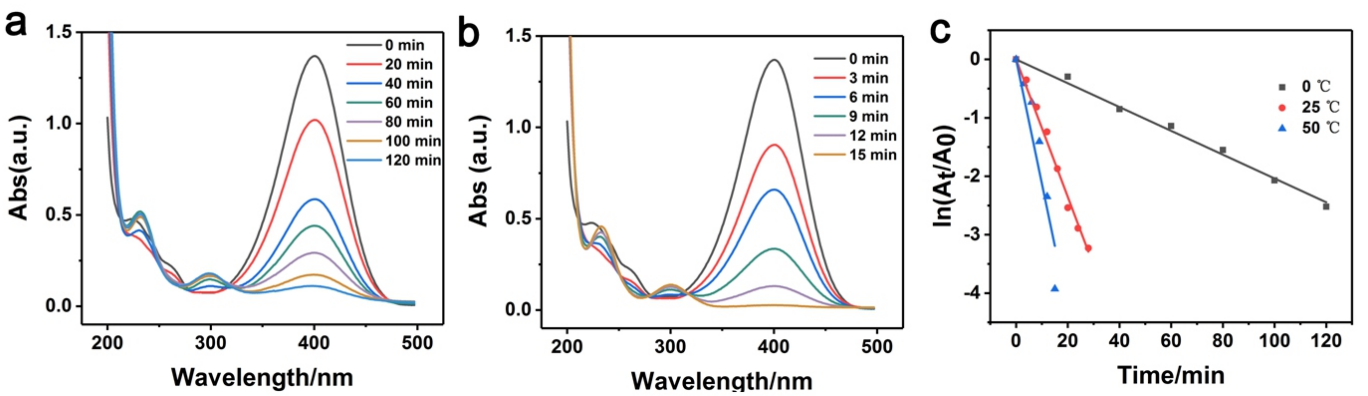

Fig. 9 UV spectrum of Au-NPs/rGO microspheres in 0.4 mol 4-NP and 48.0 mol $NaBH_4$ at (a)273 K, (b) 323 K, and the relation of t *vis* ln (A_t/A_0) (c) at 273 K, 298 K and 323 K.

the solution was centrifuged, and the supernatant was used to collect the UV spectrum. The centrifuged substrate was retained, the same amount of 4-NP and $NaBH_4$ were added, and then the same experiment was performed and repeated ten times. Fig. 10 showed the test results, and it was found that the catalytic activities were still retained at 95.1% after ten cycles. In addition, the reason for the slight loss of performance is possibly due to the incomplete centrifugation or the decreasing catalytic performance of the catalyst itself. These as prepared Au-NPs/rGO microspheres exhibited extraordinary stability as catalysts and demonstrated that our Au-NPs/rGO microsphere can be used as an ideal catalyst toward the reduction of 4-NP reaction and a potential catalytic treatment in environment protection area.

4. Conclusion

Novel Au-NPs/reduced graphene oxide microspheres composites were successfully synthesized by the spray-drying technique. The content of Au-NPs in the microspheres reached 30.3 %. These novel Au-NPs encapsulated within the rGO microsphere exhibited high catalytic activities. The catalytic properties of the Au-NPs within the rGO microspheres towards the reduction of the 4-NP to 4-AP with the presence of the $NaBH_4$ were then investigated, and it was found that first order rate constant was $K=1.96\times10^{-3}$ s^{-1}, which was measured for the catalytic reduction of 4-NP at given conditions. The activation energy of the reaction, $E_a=3.5\times10^4$ J/mol, was obtained by using the reaction rate constants at different temperatures. The as-prepared catalysts material can effectively catalyze the reduction of 4-nitrophenol to 4-aminophenol under mild reaction conditions. The stabilities of the catalytic activities of the Au-NPs within rGO microspheres were investigated and it was found that the catalytic activities were maintained 95.1% after the catalysts were used ten times. This new material exhibited potential applications for the development of novel catalytic device in environment protection and sensor system.

Conflict of interest

There are no conflicts to declare.

Acknowledgements

This work was supported by the National Natural Science Foundation of China grant (No. 21475076), International S&T collaboration Program of China (No. 2015DFA50060), Innovation and achievement transformation projects of Shandong Province (NO. 2014ZZCCX01401).

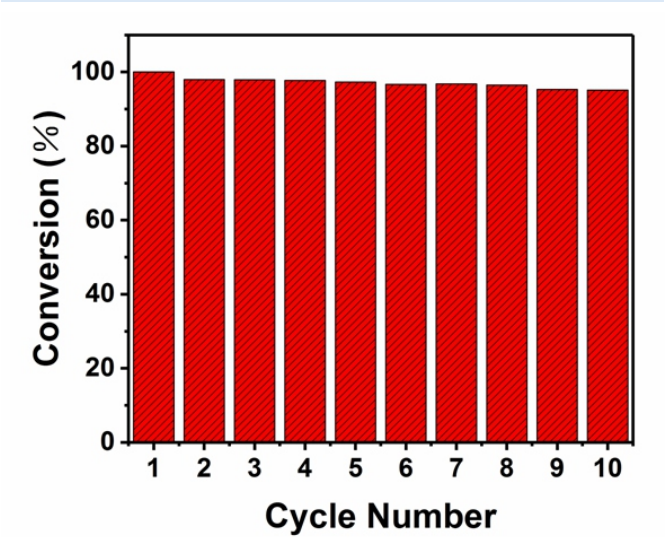

Fig. 10 The catalytic activities towards the reduction of 4-NP to 4-AP in different cycles.

Reference

1. K. Kuroda, T. Ishida and M. Haruta, *J. Mol. Catal. A-Chem,* 2009, **298**, 7-11.
2. H. Park, D. A. Reddy, Y. Kim, S. Lee, R. Ma, M. Lim and T. K. Kim, *Appl. Surf. Sci*, 2017, **401**, 314-322.
3. W. Dong, S. Cheng, C. Feng, N. Shang, S. Gao and C. Wang, *Catal. Commun,* 2017, **90**, 70-74.
4. B. Pan, W. Du, W. Zhang, X. Zhang, Q. Zhang, B. Pan, L. Lv, Q. Zhang and J. Chen, *Environ. Sci. Technol*, 2007, **41**, 5057-5062.
5. Ö. S. Kuşcu and D. T. Sponza, *Microb. Tech,* 2005, **36**, 888–895.
6. A. Nezamzadeh-Ejhieh and S. Khorsandi, *J. Ind. Eng. Chem*, 2014, **20**, 937–946.
7. P. Murugaesan, P. Aravind, N. G. Muniyandi and S. Kandasamy, *Environ. Technol*, 2015, **36**, 2618.
8. M. Blosi, S. Albonetti, A. L. Costa, N. Sangiorgi and A. Sanson, *Chem. Eng. J,* 2013, **215(2)**, 616-625.
9. R. Krishna, D. M. Fernandes, C. Dias, J. Ventura, E. V. Ramana, C. Freire and E. Titus, *Int. J. Hydrogen. Energ,* 2015, **40**, 4996-5005.
10. K. Wang, X. U. Li, H. Chen, H.Qiao , C. Chen and N. Zhang, *Chem. J. Chinese. U,* 2016, **37**, 723-727.
11. X. Cao, S. Yan, F. Hu, J. H. Wang, Y. Wan, B. Sun and Z. D. Xiao, *RSC. Adv,* 2016, **6**, 64028-64038.
12. J. Krajczewski, K. Kołątaj and A. Kudelski, *Appl. Surf. Sci,* 2016, **388**, 624-630.
13. X. Gu, W. Qi, X. Xu, Z. Sun, L. Zhang, W. Liu, X. Pan and D. Su, *Nanoscale,* 2014, **6(12)**, 6609-16.
14. J. P. Genet, *Acc. Chem. Res,* 2003, **36(12)**, 908-918.
15. S. I. Yamazaki, Y. Yamada, S. Takeda, M. Goto, T. Ioroi, Z. Siroma and K. Yasuda, *Phys. Chem. Chem. Phys*. 2016, **12**, 8968-8976.
16. Y. Zheng, J. Shu and Z. Wang, *Mater. Lett*, 2015, **158**, 339-342.
17. X. Jiang, N. Koizumi, X. Guo and C. Song, *Appl. Catal. B-Environ,* 2015, **170-171**, 173-185.
18. K. Mette, S. Kühl, A. Tarasov, H. Düdder, K. Kähler, M. Muhler, R. Schlögl and M. Behrens, *Catal. Today,* 2015, **242(242)**, 101-110.
19. J. H. Ramirez, F. J. Maldonado-Hódar, A. F. Pérez-Cadenas, C. Moreno-Castilla, C. A. Costa and L. M. Madeira, *Appl. Catal. B-Environ,* 2007, **75(3–4)**, 312-323.
20. D. A. Aguilera, A. Perez, R. Molina and S. Moreno, *ppl. Catal. B-Environ*, 2011, **(1–2)**, 144-150.
21. Y. C. Chang and D. H. Chen, *J. Hazard. Mater,* 2009, **165(1-3)**, 664.
22. J. Llorca, A. Casanovas, M. Domínguez, I. Casanova, I. Ngurell and M. Seco, O. Rossell, *J. Nanopart. Res,* 2007, **10(3)**, 537-542.
23. M. A. Centeno, M. Paulis, M. Montes and J. A. Odriozola, *Appl. Catal. B-Environ*, 2005, **61(3–4)**, 177-183.
24. H. Qi, D. Liu, L. Fei, L. Teng and F. Sun, *Rare. Metal. Mat. Eng*, 2015, **44**, 887-891.
25. A. Bhargava, N. Jain, S. Gangopadhyay and J. Panwar, *Process. Biochem*, 2015, **50**, 1293-1300.
26. A. Zhu, Y. Lu, Y. Zhou and S. Dai, *Journal of Materials Science: Materials in Medicine,* 2010, **21(12)**, 3095-101.
27. J. Yang, J. Duan ,L. Zhang, B. Lindman, H. Edlund and M. Norgren , *Cellulose*, 2016, **23(5)**, 3105-15.
28. X. Wang, J. Wang, X. Dong, F. Zhang, L. Ma, X. Fei, X. Zhang and H. Ma, *J. Alloy. Compd,* 2016, **656**, 181-188.
29. Y. Liu, H. Dai, J. Deng, L. Zhang, Z. Zhao, X. Li, Y. Wang, S. Xie, H. Yang and G. Guo, *Inorg. Chem*. 2013, **52(15)**, 8665-8676.
30. F. Dong, W. Guo, S. K. Park and C. S. Ha, *Chem. Commun*, 2011, **48**, 1108-1110.
31. A. K. Geim and K. S. Novoselov, *Nat. Mater*, 2007, **6**, 183-191.
32. S. Stankovich, D. A. Dikin, R. D. Piner, K. A. Kohlhaas, A. Kleinhammes and Y. Jia, *Carbon.* 2007, **45(7)**, 1558-65.
33. B. Vellaichamy, P. Prakash and J. Thomas, *Ultrasonics Sonochemistry*, 2018, **48**, 362-9.

34. Z. Liu, J. T. Robinson, X. Sun and H. Dai, *J. Am. Chem. Soc*, 2008, **130**, 10876-10877.
35. G. Prieto, H. Tüysüz, N. Duyckaerts, J. Knossalla , G. H. Wang and F. Schüth, *Chem. Rev*., 2016, **116(22)**, 14056-119.
36. F. Zhang, Y. Yuan, Y. Zheng, H. Wang, T. Liu and S. Hou, *Microchim. Acta,* 2017,**184**, 1565-1572.
37. M. Šimšíková, M. Bartoš, P. Keša and T. Šikola, *Mater. Chem. Phys*., 2016, **177**, 339-45.
38. B. Wang, S. Yan and Y. Shi, *J. Solid. State. Electr,* 2015, **19**, 307-314.
39. J. M. Walker and J. M. Zaleski, *Nanoscale,* 2015, **8(3)**, 1535-1544.
40. P. Zhao, X. Feng, D. Huang and G. Yang, *Coordin. Chem. Rev*, 2015, **287**, 114-136.
41. K. B. Narayanan and N. Sakthivel, *J. Hazard. Mater.,* 2011, **189**, 519-25.
42. H. Fang, M. Wen, H. Chen, Q. Wu and W. Li, *Nanoscale,* 2015, **8**, 536-542.
43. Z. Zhang, C. Shao, Y. Sun, J. Mu, M. Zhang, P. Zhang, Z. Guo, P. Liang, C. Wang and Y. Liu, *J. Mater. Chem*, 2011, **22**, 1387-1395.
44. L. F. Villalobos, P. Neelakanda, M. Karunakaran, D. Cha and K. V. Peinemann, *Catal. Today,* 2014, **236**, 92-97.
45. J. Luo, N. Zhang, R. Liu and X. Liu, *RSC. Adv,* 2014, **4**, 64816-64824.
46. Q. Wang, W. Jia, B. Liu, A. Dong, X. Gong, C. Li, P. Jing, Y. Li, G. Xu and J. Zhang, *J. Mater. Chem. A,* 2013, **1**, 12732-12741.
47. Y. Choi, H. S. Bae, E. Seo, S. Jang, K. H. Park and B. S. Kim, *J. Mater. Chem*, 2011, **21**, 15431–15436
48. T. Ji, L. Li, M. Wang, Z. Yang and X. Lu, *RSC Adv.*, 2014, **4(56)**, 29591-4.
49. S. Panigrahi, S. Basu, S. Praharaj, S. Pande, S. Jana, A. Pal, S. Kuma. R. Ghosh and P. Tarasankar , *J. Phys. Chem. C,* 2007, **111**, 4596-4605**.**